Protein Kinase A Inhibitor H89 Attenuates Experimental Proliferative Vitreoretinopathy

Yali Lyu,[1,2] Wei Xu,[3] Jieping Zhang,[1,2] Mengwen Li,[1,2] Qingyi Xiang,[2] Yao Li,[2] Tianhao Tan,[2] Qingjian Ou,[1,2] Jingfa Zhang,[4] Haibin Tian,[1,2] Jing-Ying Xu,[1,2] Caixia Jin,[1,2] Furong Gao,[1,2] Juan Wang,[1,2] Weiye Li,[5] Ao Rong,[3] Lixia Lu,[1,2] and Guo-Tong Xu[1,2,6]

[1]Department of Ophthalmology of Shanghai Tenth People's Hospital, Laboratory of Clinical Visual Science of Tongji Eye Institute, and Department of Pharmacology, Tongji University School of Medicine, Shanghai, China
[2]Department of Regenerative Medicine, and Stem Cell Research Center, Tongji University School of Medicine, Shanghai, China
[3]Department of Ophthalmology, Tongji Hospital, Tongji University School of Medicine, Shanghai, China
[4]Department of Ophthalmology, Shanghai General Hospital (Shanghai First People's Hospital), Shanghai Jiao Tong University, Shanghai, China
[5]Department of Ophthalmology, Drexel University College of Medicine, Philadelphia, Pennsylvania, USA
[6]Collaborative Innovation Center for Brain Science, Tongji University, Shanghai, China

Correspondence: Guo-Tong Xu, Department of Ophthalmology of Shanghai Tenth People's Hospital, and Laboratory of Clinical Visual Science of Tongji Eye Institute, Tongji University School of Medicine, 1239 Siping Road, Medical School Building, Room 623, Shanghai 200092, China; gtxu@tongji.edu.cn.
Lixia Lu, Department of Ophthalmology of Shanghai Tenth People's Hospital, and Lab of Clinical Visual Science of Tongji Eye Institute, Tongji University School of Medicine, 1239 Siping Road, Medical School Building, Room 708, Shanghai 200092, China; lulixia@tongji.edu.cn.
Ao Rong, Department of Ophthalmology, Tongji Hospital Affiliated to Tongji University, 389 Xincun Road, Tongkang Building, Shanghai 200065, China; rongao@163.com.

AR, LL and GTX contributed equally to the work.

Received: March 24, 2019
Accepted: November 11, 2019
Published: February 7, 2020

Citation: Lyu Y, Xu W, Zhang J, et al. Protein kinase A inhibitor H89 attenuates experimental proliferative vitreoretinopathy. *Invest Ophthalmol Vis Sci*. 2020;61(2):1. https://doi.org/10.1167/iovs.61.2.1

Purpose. This study aimed to explore the role of the protein kinase A (PKA) pathway in proliferative vitreoretinopathy (PVR) and the effect of the PKA inhibitor H89 on experimental PVR.

Methods. Epiretinal membranes (ERMs) were acquired from PVR patients and analyzed by frozen-section immunofluorescence. An in vivo model was developed by intravitreal injecting rat eyes with ARPE-19 cells and platelet-rich plasma, and changes in eye structures and vision function were observed. An in vitro epithelial-mesenchymal transition (EMT) cell model was established by stimulating ARPE-19 cells with transforming growth factor (TGF)-β. Alterations in EMT-related genes and cell function were detected. Mechanistically, PKA activation and activity were explored to assess the relationship between TGF-β1 stimulation and the PKA pathway. The effect of H89 on the TGF-β-Smad2/3 pathway was detected. RNA sequencing was used to analyze gene expression profile changes after H89 treatment.

Results. PKA was activated in human PVR membranes. In vivo, H89 treatment protected against structural changes in the retina and prevented decreases in electroretinogram b-wave amplitudes. In vitro, H89 treatment inhibited EMT-related gene alterations and partially reversed the functions of the cells. TGF-β-induced PKA activation was blocked by H89 pretreatment. H89 did not affect the phosphorylation or nuclear translocation of regulatory Smad2/3 but increased the expression of inhibitory Smad6.

Conclusions. PKA pathway activation is involved in PVR pathogenesis, and the PKA inhibitor H89 can effectively inhibit PVR, both in vivo and in vitro. Furthermore, the protective effect of H89 is related to an increase in inhibitory Smad6.

Keywords: proliferative vitreoretinopathy, protein kinase A, H89, epithelial-mesenchymal transition, transforming growth factor beta, Smad6

Proliferative vitreoretinopathy (PVR) is a common complication following rhegmatogenous retinal detachment (RD) or severe ocular trauma, and no significant advances have been made for the clinical management of this condition.[1] PVR is characterized by the formation of membranes on the surfaces of the detached retina and the posterior hyaloid. The contraction of such membranes causes retinal distortion and tractional RD.[2] The

pathogenesis of PVR includes cell migration, cell proliferation, and epiretinal membrane (ERM) formation and contraction, and the main cellular participants are retinal pigment epithelial (RPE) cells.[3,4] In RD, the blood–retinal barrier is disrupted, and the chemotactic and mitogenic activities are increased in the vitreous humor. Proliferating factors, such as transforming growth factor β (TGF-β), platelet-derived growth factor, fibroblast growth factor, epidermal growth factor, insulin-like growth factor, vascular endothelial growth factor, and hepatocyte growth factor, trigger RPE cells to proliferate and begin the epithelial-mesenchymal transition (EMT) process to participate in the formation of ERMs.[5–10] Therefore, RPE cell EMT is now recognized as a key step in PVR pathology, and EMT-regulating factors such as TGF-β could be potential targets for PVR treatment.

It has been increasingly reported that the TGF-β-induced EMT process is regulated by crosstalk between the TGF-β pathway and other signaling pathways and that protein kinase A (PKA) is an important component of the crosstalk. PKA, also known as cyclic AMP (cAMP)-dependent protein kinase, phosphorylates a wide variety of protein substrates when activated,[11] and its effects are associated with many functions, including cell growth, differentiation, extracellular matrix (ECM) production and apoptosis,[12,13] similar to those elicited by TGF-β. Studies have demonstrated that TGF-β-activated PKA phosphorylates cAMP-responsive element-binding protein (CREB) in various cells, including mesangial cells,[14,15] ML-CCl64 cells,[16] murine embryonic palate cells,[17] AML-12 murine hepatocytes,[18] and pancreatic acinar cells.[19] Such crosstalk between TGF-β and PKA has also been found to regulate fibronectin gene expression. Inhibition of PKA attenuates TGF-β-induced stimulation of CREB phosphorylation[20] and reduces fibronectin gene expression.[21] The interaction between TGF-β and PKA also plays an important role in colon cancer cell survival and metastasis by regulating survivin and XIAP signaling.[22]

Although PKA has been demonstrated to be able to regulate TGF-β-induced EMT in many cell types,[14,16–18] no study has reported the roles of TGF-β and PKA in the transformation of RPE cells or in the pathogenesis of PVR. Inspired by an unexpected finding regarding RPE cell differentiation in our laboratory, we propose that PKA plays a pivotal role in the pathogenesis of PVR and that blockade of PKA signaling should attenuate PVR. To test this hypothesis, we examined the expression of PRKACa, a catalytic (C) subunit of PKA, in ERMs from patients with PVR. In addition, we examined the effects of the selective and specific PKA inhibitor, H89, on an experimental PVR model and some TGF-β/PKA-related signaling endpoints under various conditions. The results showed that PKA was activated in the ERMs and H89 attenuated PVR both in vivo and in vitro. Based on the results, we propose a possible mechanism for PVR pathogenesis and suggest that PKA could be a new therapeutic target for PVR.

Materials and Methods

Reagents and Antibodies

The PKA inhibitor H89 was purchased from Selleck (Houston, TX), and human recombinant TGF-β1 and TGF-β2 were purchased from R&D Systems (Minneapolis, MN). Primary antibodies against the following proteins were used for Western blotting (WB) and immunofluorescence (IF): alpha-smooth muscle actin (α-SMA) and cytokeratin 8 (CK8) (Abcam); fibronectin, PRKACa, N-cadherin, and Gapdh (Protein Tech Group, Wuhan, China); ZO-1 (Invitrogen); CREB, phospho-CREB, Smad2/3, and phospho-Smad2/3 (Cell Signaling Technology, Carlsbad, CA); Smad6 (Novus, Danvers, MA); and Smad7 (R&D Systems, Minneapolis, MN). For WB analysis, secondary antibodies conjugated to horseradish peroxidase against rabbit or mouse immunoglobulin (Protein Tech Group, Wuhan, China) were used at a dilution of 1:5000. For IF analysis, an anti-rabbit or anti-mouse Cy3 (Jackson ImmunoResearch, West Grove, PA) antibody was used at a dilution of 1:500.

Study Approval

All patients were fully informed about this study and provided signed consent. Patients with severe systemic diseases, such as cancer and autoimmune diseases, were excluded. The study followed the guidelines of the Declaration of Helsinki and was approved by the Ethics Review Board of Tongji Hospital, Tongji University.

Human PVR Membrane Frozen Sections

Human PVR membranes were obtained during vitreoretinal surgeries from patients with RD complicated with PVR (Tongji Hospital, Tongji University, Shanghai, China). The specimens were maintained in physiological saline and then fixed in 4% paraformaldehyde overnight at 4°C. After being embedded and frozen, the samples were sectioned at a thickness of 8 µm with a freezing microtome (Leica, Germany).

Experimental Animals

All experimental animals were treated in accordance with the Association for Research in Vision and Ophthalmology Statement for the Use of Animals in Ophthalmic and Vision Research and the Guidelines for the Care and Use of Animals (National Research Council and Tongji University). Normal adult male Sprague-Dawley (SD) rats aged 6 to 8 weeks and weighing 160 to 180 g (Slaccas, China) were used for this experiment.

Cell Culture and Treatment

The human RPE cell line ARPE-19 (CRL-2302; American Type Culture Collection) was cultured in RPE medium consisting of DMEM/F-12 containing 10% fetal bovine serum (FBS) (both from Gibco) and 1% penicillin-streptomycin (Beyotime, China), at 37°C and 5% CO_2, and the medium was refreshed every 2 to 3 days. For the in vivo PVR model, just before intravitreal injection, ARPE-19 cells were collected and resuspended in sterile pyrogen-free phosphate-buffered saline (PBS) or platelet-rich plasma (PRP). For in vitro EMT induction, cells were starved in serum-free medium overnight before being treated with 10 ng/mL TGF-β1 or TGF-β2 with or without H89.

Preparation of PRP

PRP was collected as previously described.[23,24] Blood was collected into ethylene diamine tetraacetic acid vacuum tubes from the tail veins of SD rats. The samples were centrifuged at 180*g* for 5 minutes to separate the PRP (supernatant) from the erythrocytes and leukocytes. The PRP was transferred into a clean tube, centrifuged at 200*g* for 10 minutes and then preserved on ice for approximately 10 minutes until intravitreal injection.

Investigative Ophthalmology & Visual Science

Intravitreal Injection of ARPE-19 Cells, PRP, and H89

Experimental PVR models were constructed as previously reported, with slight modifications.[23] For PVR model preparation, SD rats were intravitreally injected with ARPE-19 cells and PRP. Color photographs of the fundus were obtained using an APS-AER camera (Kanghuaruiming S&T, China) on days 7, 14, 21, and 28 postinjection (PI) to confirm the successful establishment of the PVR model. Then, 21 rats were divided equally into three groups, each of which received intravitreal injections of either PBS, ARPE-19 cells + PRP, or ARPE-19 cells + PRP + H89. The rats were anesthetized by intraperitoneal injection with 2% pentobarbital sodium (40 mg/kg) plus an intramuscular injection of Sumianxin (0.5 mL/kg) for general anesthesia; tropicamide/phenylephrine eye drops were used for pupil dilation, and tetracaine eye drops were used for local anesthesia. Then, the eyes were gently protruded using a rubber ring filled with a viscoelastic substance, and a self-sealing wound tunnel was created using a 1.5-cm 28-gauge needle 1 mm posterior to the corneal limbus. After the vitreous cavity collapsed because of the outflow of vitreous fluid, a blunt 32-gauge Hamilton syringe was introduced through the sclera into the vitreous cavity under a surgical microscope (SM-J, Eder, China). Then, 8 µL of PBS, 4 µL of PRP containing ARPE-19 cells (2.4×10^6) plus 4 µL of PBS or 4 µL of PRP containing ARPE-19 cells (2.4×10^6) plus 4 µL of H89 diluted in PBS was injected into the eyes of the separate groups. The final concentration of H89 was 10 µM. Four rats in the PVR group were excluded because they developed cataracts 1 week PI.

Electroretinogram Examination

The b-wave amplitude was measured by an electroretinogram (ERG) recording on days 7, 14, 21, and 28 PI using an AVES-2000 electrophysiological apparatus (Kanghuaruiming S&T). The rats were placed in a dark room overnight for dark adaption before the ERG test. The rats were anesthetized as described previously. The corneas of the rats were coated with a modestly conductive paste. A ground electrode was implanted into the subcutaneous part of the tail root of each rat. The positive electrode was placed subcutaneously between the ears, and the negative electrodes were contacted on the surfaces of the corneas. The two eyes were simultaneously stimulated twice with a bright flash intensity of 0.06325 cds/m, which allowed the responses of the photoreceptors to be recorded.

IF Staining and Imaging

Rat eye samples were dissected, fixed in 4% paraformaldehyde in PBS, embedded, frozen, and sectioned at a thickness of 8 µm along the vertical meridian of the eyeball through the optic nerve head. All samples were stained with the indicated primary antibodies at 4°C overnight and with secondary antibodies for 1 hour at room temperature. The slides were mounted with 4′,6′-diamidino-2-phenylindole dihydrochloride (DAPI) (Sigma), blocked in fluorescent mounting medium (DAKO, Denmark), and then analyzed using a confocal microscope (Nikon, Japan).

Protein Extraction and WB

Total proteins of rat retinas or cells were extracted using RIPA buffer (Beyotime, China) containing 1% phenylmethylsulfonyl fluoride (Sigma). The protein concentration was quantified using a Pierce BCA Protein Assay Kit (Thermo Scientific). The proteins were fractionated by sodium dodecyl sulfate–polyacrylamide gel electrophoresis and transferred to PVDF membranes. The membranes were blocked, incubated with primary antibodies overnight at 4°C, and then incubated with secondary antibodies at room temperature for 1 hour. The immune complexes were detected with an automatic chemiluminescence analysis system (Tanon, China). Analysis of each protein band was performed using ImageJ software. The expression of glyceraldehyde 3-phosphate dehydrogenase (GAPDH) was used as an internal control.

RNA Extraction and Quantitative Real-Time Polymerase Chain Reaction

The cells were collected with TRIzol (TaKaRa, Japan). Total RNA was extracted, and reverse transcription was performed using PrimeScript RT Master Mix (TaKaRa, Japan). Quantitative real-time polymerase chain reaction (RT-qPCR) was performed in a Bio-Rad CFX Manager 2.1 Detection System (Bio-Rad) using Real MasterMix (SYBR Green) (Tiangen Biotech, China). RT-qPCR amplification was performed in duplicate (the program was as follows: denaturation at 95°C for 15 minutes followed by 40 cycles of 95°C for 10 seconds and 60°C for 40 seconds). All primer sequences are listed in Table 1. The messenger RNA (mRNA) expression was normalized to that of Gapdh.

Scratch Assay

Cells were treated with the indicated agents after the middles of the wells were scratched with pipette tips. Images were obtained under a light microscope (Zeiss, Germany) 24 and 48 hours later to measure the width of the scratches. The gap sizes were measured and compared with those of the original scratches, and the values are expressed as the scratch area ratio.

Transwell Assay

Cells were treated with different agents. Then, 1×10^5 cells in 100 µL of DMEM/F12 containing 0.5% FBS were seeded into the upper compartment of an 8-mm pore transwell system (Corning), whereas 600 µL of DMEM/F12 containing 10% FBS was added to the lower compartment in a 24-well plate. After a 24-hour period of migration, the nonmigratory cells were removed from the upper membrane, whereas the migratory cells attached to the bottom surface of the membrane were fixed with methanol for 20 minutes and stained with eosin for an additional 20 minutes at room temperature. Images were obtained using a phase contrast microscope (Olympus Corporation, Japan), and the cells were counted using NIH ImageJ software.

Collagen Gel Contraction

ARPE-19 cells pretreated with TGF-β1 with or without H89 for 48 hours were harvested and suspended in DMEM/F12 with 10% FBS and Collagen I (Gibco) (final concentration,

Investigative Ophthalmology & Visual Science

Table 1. The PCR Primer Sequence

Gene	Forward Primer (5′-3′)	Reverse Primer (5′-3′)
Gapdh	AGGTCGGTGTGAACGGATTTG	TGTAGACCATGTAGTTGAGGTCA
ZO-1	ATTGTCGTCGCATGTAGATCC	GGGTTCATAGGTCAGATTAGGC
a-SMA	AATGCAGAAGGAGATCACGG	TCCTGTTTGCTGATCCACATC
N-Cadherin	CCCAAGACAAAGAGACCCAG	GCCACTGTGCTTACTGAATTG
PRKACa	CCCTGAGATTATCCTGAGCAAAG	TCGTTGACCCCATTCTTGAG

3.36 mg/mL). Mixtures of 10 × DMEM/F12, cell suspension (final cell density, 2.5×10^5 cells/well), sterile distilled water, and sterile 1N NaOH were prepared and mixed on ice. A total volume of 0.5 mL of the mixture was added to each well, and the plates were incubated for 1 hour at 37°C under 5% CO_2 to promote gel polymerization. The gels were freed from the sides with pipette tips, and serum-free DMEM/F12 (0.5 mL) containing the indicated agents was then added on top of the gel. Photographs were taken after 48 hours to enable quantitation of the gel contraction length ratios using ImageJ software, and the contraction areas were calculated and analyzed.

PKA Activity Assay

PKA kinase activity was analyzed using a PepTag Assay for Non-Radioactive Detection of cAMP-Dependent Protein Kinase (Kemptide [LRRASLG]; Promega) according to the manufacturer's instructions. Confluent cells grown in 60-mm dishes were starved overnight and then treated with TGF-β1 for the indicated durations and at the indicated concentrations. The cells were lysed on ice in extraction buffer that included a protease inhibitor cocktail and phenylmethylsulfonyl fluoride. The cell lysates were homogenized by sonication. The cell debris was removed by centrifugation, and the supernatants were incubated for 30 minutes at room temperature with PepTag A1 peptide. The reaction was stopped by heat inactivation on a 95°C heating block for 10 minutes. Then, the samples were loaded onto a gel (0.8% agarose solution in 50 mM Tris-HCl, pH 8.0) and electrophoresed at 120 V until band separation was apparent. Then, the gel was examined under ultraviolet light. To quantitate the kinase activity, the charged phosphorylated bands were excised from the gel in a uniform total volume of approximately 250 µL. The gel slices were heated at 95°C until the gel melted, and 125 µL of the hot agarose was transferred to a tube containing 75 µL of Gel Solubilization Solution (which had been warmed to room temperature and mixed well) and 50 µL of glacial acetic acid. The solution (250 µL) was quickly vortexed and transferred to a well in a 96-well plate. The absorbance at 570 nm was measured. The blank sample for the plate reader was liquefied agarose without PepTag Peptide. Forskolin, an activator of the PKA pathway,[25] was used as a positive control.

Nuclear and Cytoplasmic Separation

NE-PER Nuclear and Cytoplasmic Extraction Reagents (Thermo) were used for nuclear and cytoplasmic fractionation according to the manufacturer's instructions. ARPE-19 cells were harvested and transferred to 1.5-mL microcentrifuge tubes. The supernatants were discarded, and the cell pellets were left to dry as much as possible. Ice-cold Cytoplasmic Extraction Reagent (CER) I was added, and the cell pellets were resuspended. The tubes were incubated on ice for 10 minutes. Ice-cold CER II was then added to the tubes, which were vortexed and incubated on ice for 1 minute. The tubes were again vortexed and centrifuged for 5 minutes at maximum speed in a microcentrifuge (~16,000*g*). The supernatant (cytoplasmic extract) was immediately transferred to clean prechilled tubes. The insoluble (pellet) fractions, which contained the nuclei, were resuspended in ice-cold Nuclear Extraction Reagent and vortexed. The samples were then placed on ice and vortexed for 15 seconds every 10 minutes for a total of 40 minutes. The tubes were centrifuged at maximum speed (~16,000*g*) in a microcentrifuge for 10 minutes, and the supernatant (nuclear extract) was immediately transferred into clean prechilled tubes. The extracts were stored at -80°C until use. The CER I:CER II: Nuclear Extraction Reagent volume ratio was 200:11:100.

RNA Sequencing and Kyoto Encyclopedia of Genes and Genomes Signaling Pathway Enrichment Analysis

Three groups of samples were subjected to RNA sequencing: the control group included ARPE-19 cells without any treatment, the TGF-β1 group was treated with only TGF-β1, and the TGF-β1+H89 group was pretreated with H89 and then treated with TGF-β1 for 48 hours. Total RNA sample quality control for the three groups was conducted with an Agilent 2100 Bioanalyzer (Agilent RNA 6000 Nano Kit). All the low-quality reads (reads in which more than 20% of the bases have a quality lower than 10), reads with adaptors and reads with unknown bases (more than 5% N bases) were filtered out to obtain the clean reads. The selected reads were assembled into Unigenes and were subjected to Unigene functional annotation and simple sequence repeat detection; then, the Unigene expression levels and single-nucleotide polymorphisms of each sample were calculated. Differentially expressed genes (DEGs) were identified with PossionDis (parameters: a fold change $\geq$2.00 and a false discovery rate [FDR] $\leq$0.001). DEGs between samples were identified and assayed by clustering analysis and functional annotation. The DEGs were classified by their official Kyoto Encyclopedia of Genes and Genomes (KEGG) classifications, and pathway functional enrichment analysis was performed using the phyper package in R. The FDR was calculated for each *P* value, and in general, terms with an FDR not larger than 0.01 were defined as significantly enriched. RNA sequencing experiments were conducted by the Beijing Genomics Institute in China.

Statistical Analysis

The data are expressed as the mean ± standard error of the mean (SEM), as indicated. The data were analyzed using GraphPad Prism 6.0 (GraphPad Software). Statistical analyses were conducted with Student's *t*-test. For all analyses, a

Investigative Ophthalmology & Visual Science

Table 2. Basic Patient Information

Number	Sex	Age/Years	Eye	Major Diagnosis	Other Diagnosis
P01	Female	67	Left	PVR	Age-related cataracts After intraocular lenses implantation Coronary atherosclerotic heart disease
P02	Male	75	Right	PVR	Rhegmatogenous retinal detachment Macular degeneration After intraocular lenses implantation Coronary atherosclerotic heart disease Atrial fibrillation Hypertension
P03	Female	59	Right	PVR	Retinal tear Age-related cataracts
P04	Female	64	Left	PVR	After vitrectomy After intraocular lenses implantation High myopia Hypertension

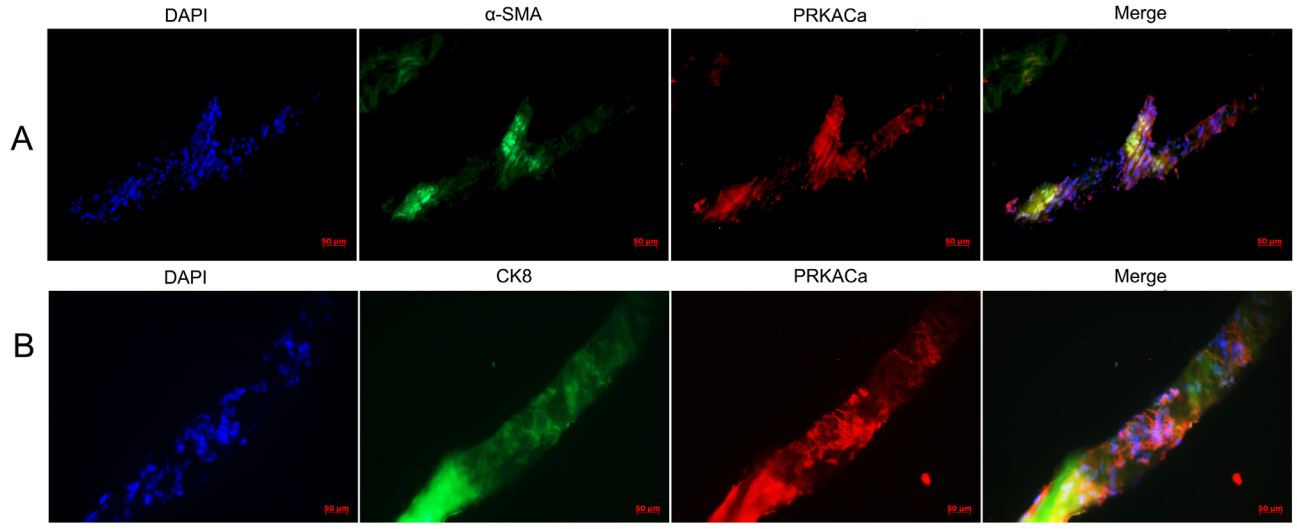

Figure 1. Coexpression of PRKACa, EMT markers, and epithelial markers in human PVR membranes. (**A**) Representative confocal pictures of double-stained human PVR membrane samples by α-SMA (green) and PRKACa (red). (**B**) Double-labeled CK8 (green) and PRKACa (red) in human PVR membranes. The blue signal represents the nuclear staining by DAPI. Original magnifications: 200×. Scale bar: 50 µm.

P value < 0.05 was considered to indicate statistical significance.

Results

Expression of PRKACa in ERMs From Patients With PVR

To investigate whether the PKA pathway is involved in the pathogenesis of PVR, we collected ERMs from patients with PVR and conducted IF to detect the expression of PRKACa, a PKA C subunit. The basic information for each patient is listed in Table 2. As shown in Figure 1, PRKACa was evidently expressed in these ERM samples from PVR patients and was partially located in the nucleus, indicating that the PKA pathway was activated in PVR membranes. In addition, PRKACa colocalized strongly with both the EMT marker α-SMA and the epithelial marker CK8. Because RPE cells were the only epithelial cells in PVR membranes, these findings suggest that PKA is activated in RPE cells, which undergo EMT and participate in the pathogenesis of PVR.

H89 Attenuated PVR and Protected Visual Function in Experimental Rats

The rat PVR model was established by intravitreal injection of ARPE-19 and PRP, and confirmed by fundus examination. Compared with normal control rats (Figs. 2A, 2B), 22 model rats exhibited different grades of PVR at different times (4 rats were excluded because of cataracts), with signs including intravitreal proliferation, ERM formation with mild retinal folds (Fig. 2C), tortuous retinal vessels, detachments, and dense membranes (Fig. 2D). These changes were obviously attenuated in the H89-treated group (Figs. 2E, 2F), indicating that H89 could ameliorate PVR in experimental rats. Functionally, as reflected in the ERG recordings (Figs. 2G, 2H), the trends of the 3 groups at 1, 2 and 3 weeks were consistent, and the generally decreased b-wave amplitudes were caused by injury due to the eye injections. At 3 weeks, the representative b-wave amplitudes in the PBS, ARPE-19 + PRP, and ARPE-19 + PRP + H89 groups were 340.6 ± 107.0 µV, 69.5 ± 15.0 µV, and 204.1 ± 45.5 µV, respectively. Compared with the ARPE-19 + PRP group, the

Investigative Ophthalmology & Visual Science

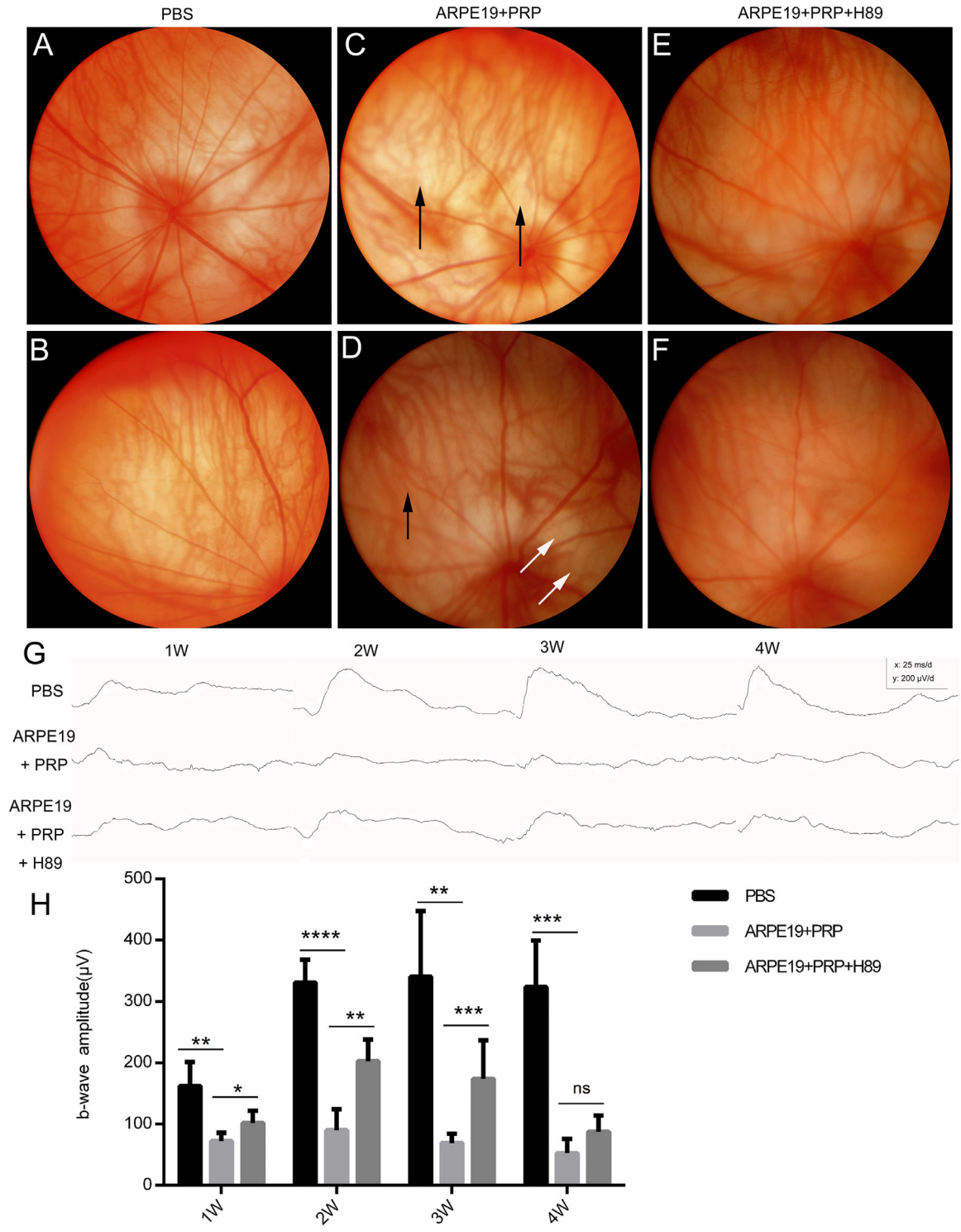

Figure 2. H89 attenuated PVR and protected visual function in experimental rats. (**A, B**) PBS control group, no proliferation. (**C, D**) PVR group, treated with ARPE-19 + PRP, intravitreal proliferation and ERM formation with mild retinal folds (black arrow in [**C**]), tortuous retinal vessels (black arrow in [**D**]), white dense membrane covering the retina and localized RDs (white arrow in [**D**]). (**E, F**) H89 intervention group, the PVR characters in (**C**) and (**D**) were obviously attenuated. (**G**) Representative ERG b-waveforms recorded at different time points (the calibration indicates 200 μV vertically and 25 ms horizontally.) (**H**) Quantitative analysis of ERG b-wave amplitudes in SD rats treated with PBS, ARPE-19 + PRP, or ARPE-19 + PRP + H89 at weeks 1, 2, 3, and 4 after intravitreal injection. Data are given as the mean ± SEM (n = 6; *$P < 0.5$; **$P < 0.1$; ***$P < 0.005$; ****$P < 0.001$).

Investigative Ophthalmology & Visual Science

ARPE-19 + PRP + H89 group exhibited a rescued b-wave amplitude, confirming that H89 also protected visual function in the PVR model rats. The protective effect of H89 lasted for 3 weeks since the effect was lost at 4 weeks ($P = 0.101$).

H89 Attenuated EMT and ERM Formation in the PVR Rat Model and in the ARPE-19 Cell Model

To further elucidate the effects of H89 on PVR and EMT, the levels of two EMT-related markers, α-SMA and fibronectin, were examined by IF in PVR models at 1 and 4 weeks PI and by WB analysis in retinas at 4 weeks PI. As shown in Figures 3A and 3B, at 1 week PI, both α-SMA and fibronectin were clearly detected in ARPE-19 + PRP-treated rats, whereas no α-SMA and fibronectin could be observed in the rats also treated with H89. At 4 weeks PI, the expression of α-SMA and fibronectin was dramatically increased, and ERM was observed. The retinal structure was disrupted, especially in the outer nuclear layer and inner nuclear layer. The expression of α-SMA and fibronectin was obviously lower in the H90-treated group compared with that in the ARPE-19 + PRP group, and the disruption in the retina was alleviated. The IF results at 4 weeks PI were further confirmed by WB examination (Figs. 3C-3E). These data demonstrated that inhibition of EMT by H89 contributed to the protective effect of H89 in the rat PVR model.

To confirm the protective effects of H89 observed in the model rats, we used an in vitro PVR model with RPE cells. As shown in Figures 3F-3H, TGF-β induced an evident decrease in the epithelial marker ZO-1 and increases in the mesenchymal markers α-SMA, N-cadherin, and fibronectin. In this system, all the TGF-β1- or TGF-β2-induced changes in both the mRNA and protein levels were evidently prevented by H89 treatment (Figs. 3F-3H). Because the effects of TGF-β1 and TGF-β2 in ARPE-19 cells were similar, as determined by RT-qPCR, TGF-β1 was predominantly used in the following study. H89 was further confirmed to alleviate TGF-β1-induced cytoskeletal remodeling and tight junction disruption, as shown by confocal IF images of rhodamine-phalloidin and ZO-1 (Fig. 3I). These results suggested that H89 could inhibit PVR-related changes in vitro as well as in vivo.

H89 Attenuated TGF-β-Induced RPE Migration and Collagen Gel Contraction

To obtain more evidence on the protective effects of H89 in PVR, we next examined the functions of RPE cells under TGF-β stimulation using a scratch assay and a transwell migration system. As shown in Figures 4A and 4C, in the scratch assays, 10 ng/mL TGF-β1 was found to enhance the migration and proliferation of RPE cells into the wound area, but these effects were significantly attenuated by the treatment of 10 μM H89 in a time-dependent manner. In the transwell system, the numbers of migrated cells were evidently increased under TGF-β1 stimulation, but such increase was significantly reduced by H89 treatment (Figs. 4B, 4D). Furthermore, based on a report that exposure of RPE cells to proinflammatory cytokines causes PVR membrane contraction, we tested the inhibitory effect of H89 on PVR by examining RPE cell collagen gel contraction. ARPE-19 cells were pretreated with TGF-β1 or TGF-β1 + H89 and then cultured in medium containing collagen. TGF-β1 induced obvious gel contraction, as qualified by the gel sizes. The TGF-β1-treated gels were 59.89 ± 3.89% of the size of the control gels, whereas H89 treatment maintained the gels at 71.73 ± 3.01% of the same control gels (Figs. 4E, 4F). These results implied that H89 could inhibit the TGF-β1-induced contraction capacity of RPE cells.

H89 Inhibited TGF-β1-Induced PKA Pathway Activation in Cultured ARPE-19 Cells

To elucidate the mechanism of action of H89 in alleviating PVR development, especially with regard to RPE cell migration, we examined PKA signaling under TGF-β1 treatment with or without H89. As shown in Figures 5A and 5B, in the process of TGF-β-induced EMT, expression of PRKACa was significantly increased, and PRKACa was found to translocate from the cytosol to the nucleus. In addition, in the TGF-β1-induced in vitro PVR model, CREB was phosphorylated, as detected by WB and IF. Furthermore, the PKA pathway could be directly activated by TGF-β1 in a dose-dependent manner (at concentrations $\leq$10 ng/mL) within 30 minutes (Figs. 5C and 5E). At a concentration of 10 ng/mL, PKA activity increased by 4 folds within 30 minutes and then decreased (Figs. 5D and 5F). On the other hand, as expected, H89 effectively blocked TGF-β1-induced PKA activation in this in vitro system. As shown in Figures 5G and 5H, the release and translocation of C subunits to the nucleus were induced by TGF-β1 but significantly blocked by H89. H89 also inhibited the phosphorylation of CREB, as examined by IF and WB. These results indicated that the PKA pathway might be activated by TGF-β stimulation, like the situation in PVR, and that such PKA activation could be blocked by PKA inhibitors, such as H89.

TGF-β-Induced PKA Activation Was Dependent on Smad6 But Not on Smad2/3

Considering that Smads are the main signal transducers for TGF-β receptors in the regulation of cell development and growth, we wondered if they are also involved in the inhibitory effects of H89 on TGF-β-induced PVR or RPE cell EMT. Therefore, we first examined changes in the canonical Smad2/3-TGF-β pathway because Smad2/3 has been reported to regulate TGF-β in several cell types and might also be associated with TGF-β in RPE cells. Unexpectedly, H89 did not affect canonical Smad2/3 signaling, as Smad2/3 expression and phosphorylation did not significantly change, even though these proteins have been reported to be completely inhibited by the TGF-β inhibitor SB431542[26] (Figs. 6A and 6B). Because Smad2/3 translocates into the nucleus when activated, nucleocytoplasmic separation was examined. The results were consistent with the WB results: both SB431524 and SIS3, a specific Smad3 inhibitor, abolished Smad2/3 translocation, whereas H89 had no effect (Fig. 6C). Such observations were further confirmed by immunoprecipitation examination of the direct relationship between PKA and Smad2/3. No difference was detected between lysed TGF-β and TGF-β+H89-treated RPE cells (Supplementary Fig. S1). These results indicated that inhibition of TGF-β-induced PKA activation was not directly dependent on the canonical Smad2/3 pathway. In addition, forskolin could not activate the Smad2/3 pathway (Fig. 6A).

Based on RNA sequencing data, the DEGs between the TGF-β1-treated RPE cells with or without 48-hour H89 treatment were identified, and the signaling pathways were

Investigative Ophthalmology & Visual Science

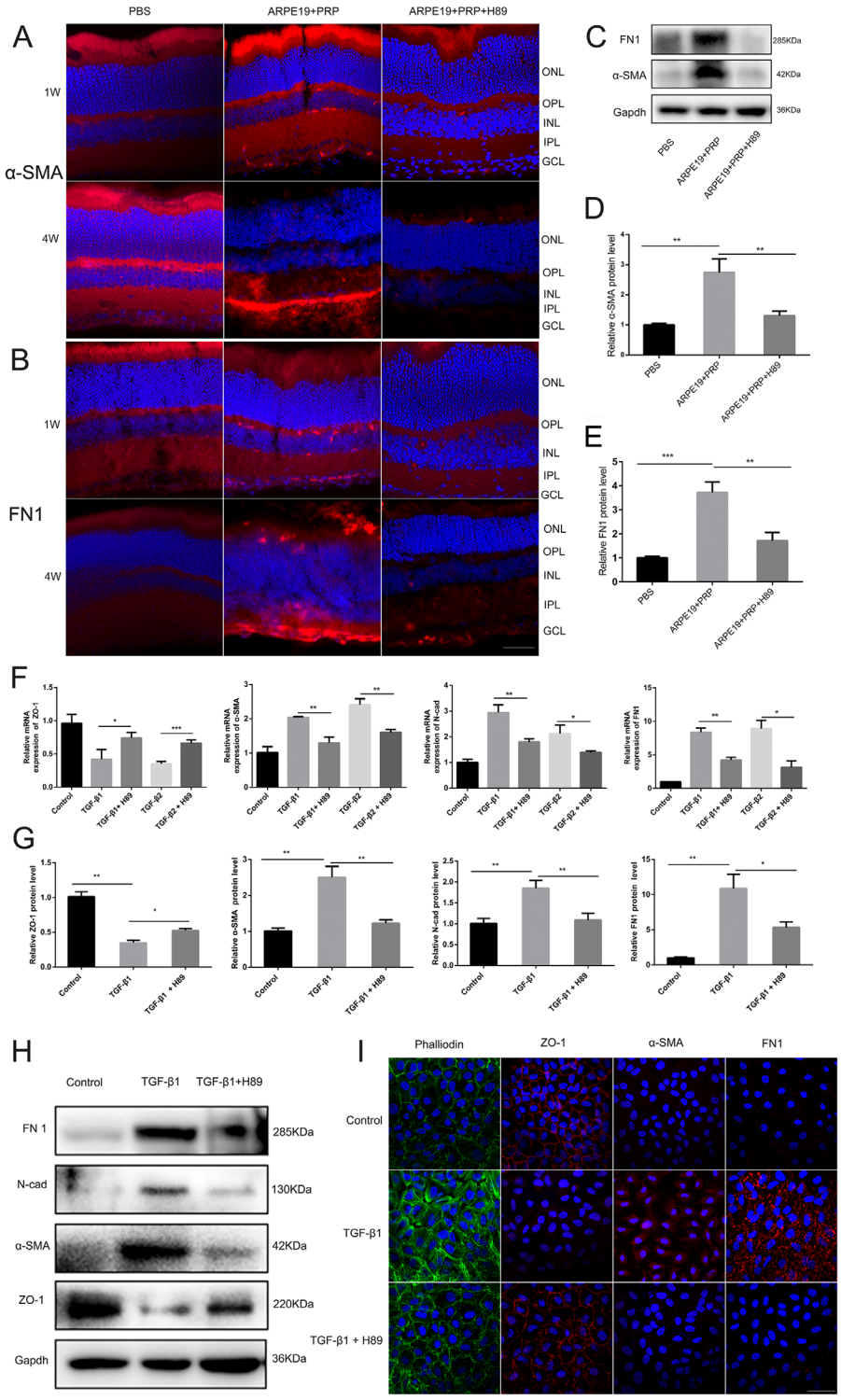

Figure 3. H89 attenuated EMT and ERM formation in a PVR rat model and in an ARPE-19 cell model. (**A, B**) Representative confocal immunofluorescence images of the EMT genes α-SMA and fibronectin in eyeball frozen sections at 1 and 4 weeks after intravitreal injection. Original magnification: 400×, oil. Scale bar: 50 µm. (**C**) Western blot analysis of α-SMA and fibronectin in the retina at 4 weeks after injection. Gapdh was used for normalization. (**D, E**) Quantification of relative protein expression in Western blots by determining their grayscale value. The data are presented as mean ± SEM (n = 3/group, $^{**}P < 0.01$, $^{***}P < 0.005$). (**F**) The mRNA levels of ZO-1, α-SMA, N-cadherin, and fibronectin were detected by RT-qPCR in ARPE-19 cells. The data are presented as mean ± SEM (n = 3/group, $^{*}P < 0.05$, $^{**}P < 0.01$). (**G**) Quantification of relative protein expression in Western blots by determining their grayscale value. The data are presented as the mean ± SEM (n = 3/group, $^{*}P < 0.05$, $^{**}P < 0.01$). (**H**) Western blot analysis of ZO-1, α-SMA, N-cadherin, and fibronectin. Gapdh was used for normalization. (**I**) Immunofluorescence analysis of rhodamine-phalloidin (actin fibers-green), ZO-1, α-SMA, and fibronectin (red) in RPE cells treated with 10 ng/mL TGF-β1 with or without H89 for 48 hours. Nuclei were stained with DAPI (blue). Slides were examined by confocal microscopy. Original magnification: 600×, oil. Scale bar: 50 µm.

Investigative Ophthalmology & Visual Science

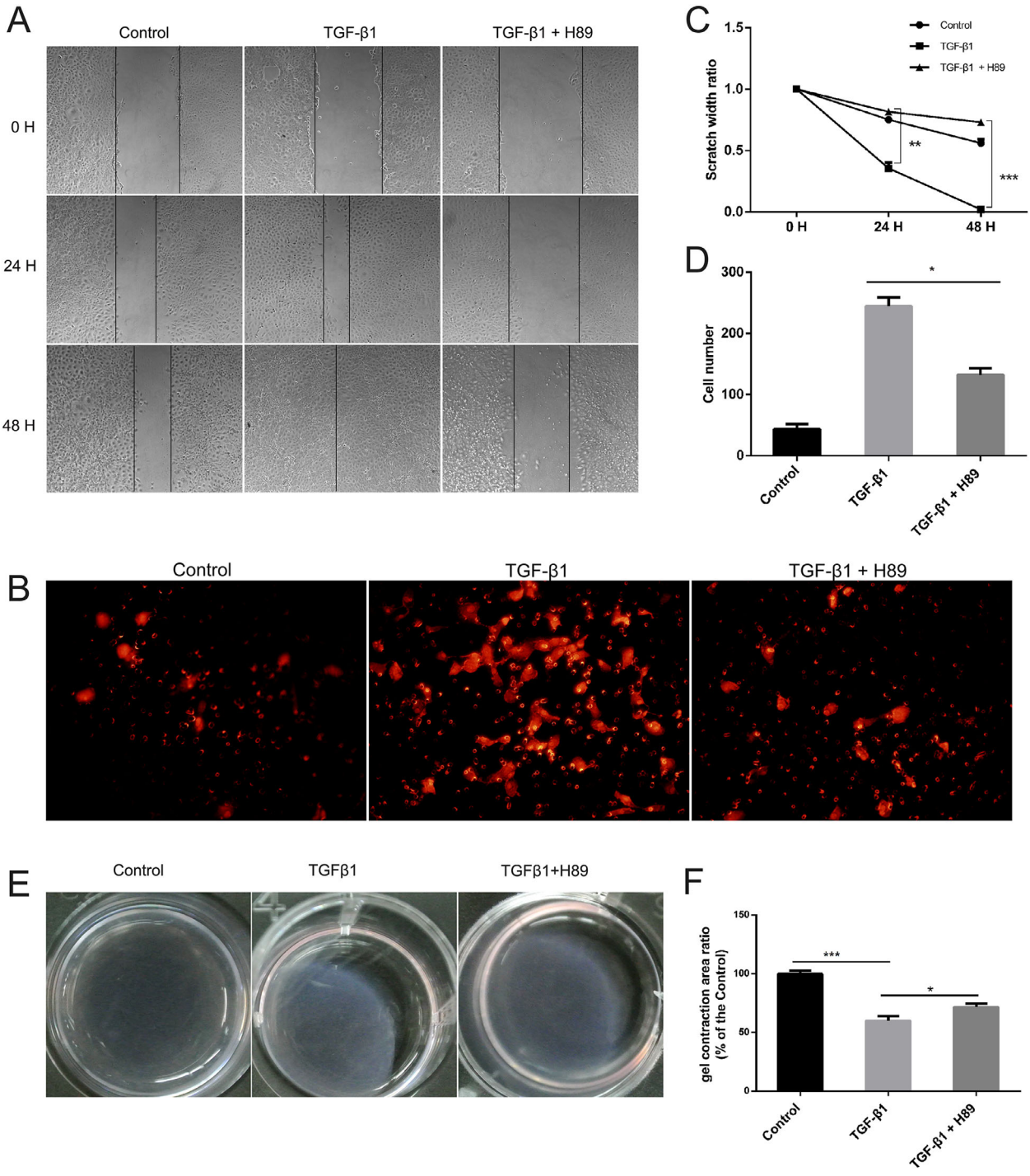

Figure 4. H89 attenuated TGF-β-induced RPE migration and collagen gel contraction. Pretreated ARPE-19 cells were cultured with or without H89 for 24 hours, and then a scratch was made followed by treatment with 10 ng/mL TGF-β1 plus H89 for an additional 48 hours. (**A**) The images were taken at 0, 24, and 48 hours after the scratch. Original magnification: 100×. (**B**) Harvested cells were allowed to migrate in the 0.8 µm transwell system for an additional 24 hours. Images were acquired under fluorescence microscopy. Original magnification: 200×. (**C**) The width of the scratch at different times; that at 0 hours was used as the control. TGF-β1-induced migration was attenuated significantly by H89 in ARPE-19 cells (n = 3/group, $^{**}P < 0.01$, $^{***}P < 0.005$). (**D**) The number of migrated cells. The data represent the average of three independent experiments and are presented as mean ± SEMs. Images of six fields were taken from each chamber ($^{*}P < 0.05$). (**E**) Representative image of collagen gel contraction for 48 hours. (**F**) The area of the gel was quantified. The data are presented as mean ± SEMs. The experiments were repeated for three times. $^{*}P < 0.05$, $^{***}P < 0.005$.

Investigative Ophthalmology & Visual Science

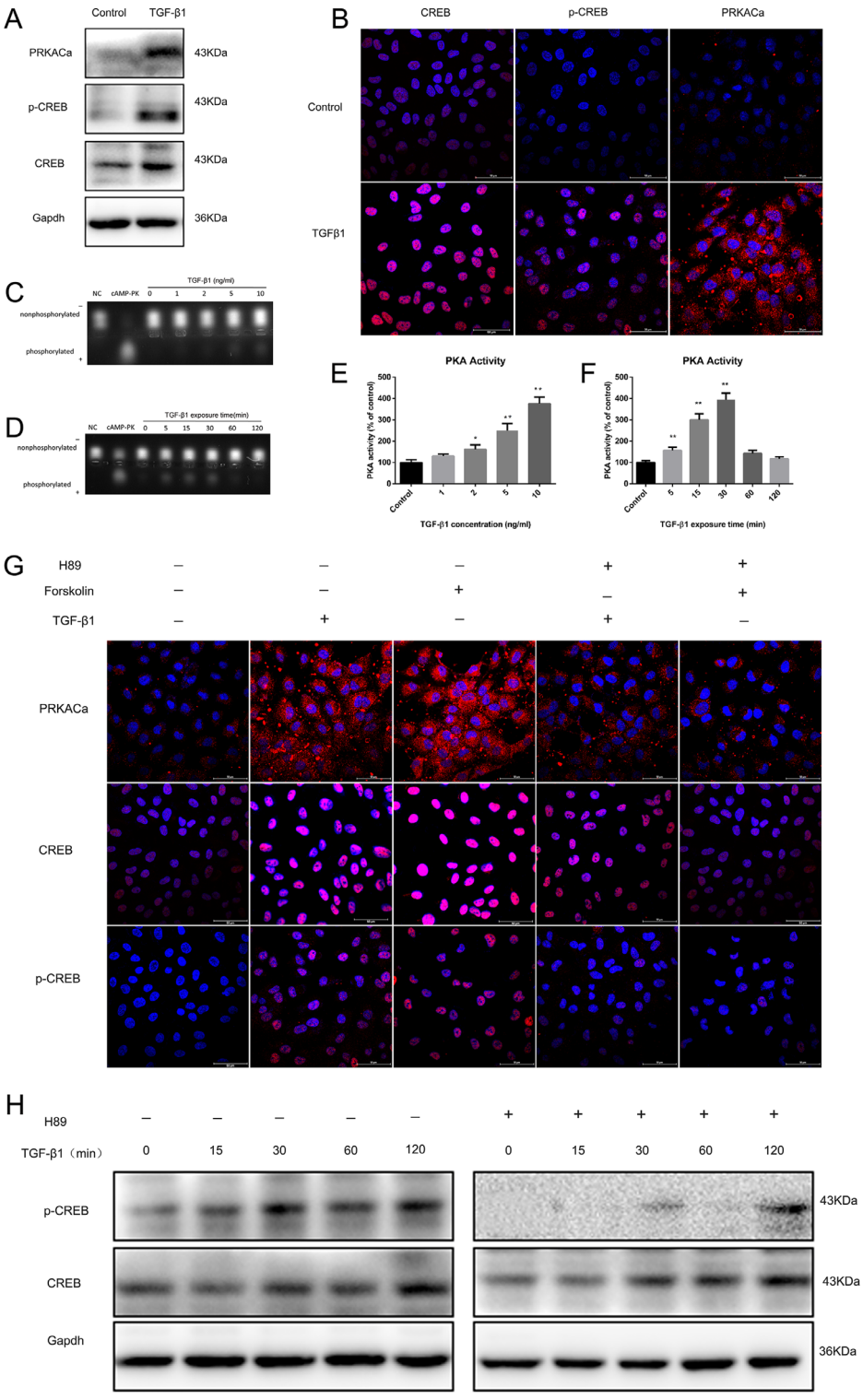

Figure 5. H89 inhibited TGF-β1-induced PKA pathway activation in cultured ARPE-19 cells. (**A**) Western blot analysis of CREB, p-CREB, and PRKACa. Gapdh was used for normalization. (**B**) Immunofluorescence analysis of CREB, p-CREB, and PRKACa (red) in RPE cells treated with 10 ng/mL TGF-β1 for 48 hours. Nuclei were stained with DAPI (blue). Slides were examined by confocal microscopy. Original magnification: 600×, oil. Scale bar: 50 µm. (**C–F**) TGF-β increased PKA activity. RPE cells were serum starved overnight and then treated with TGF-β1 at the indicated doses for 30 minutes (**C, E**) or for the indicated time periods at 10 ng/mL (**D, F**). These data were from three separate experiments and the results are expressed as increases over the control (*$P < 0.05$; **$P < 0.01$, as compared with the control). (**G**) Immunofluorescence analysis of PRKACa, CREB, and p-CREB in ARPE-19 cells treated with 10 ng/mL of TGF-β1 or 10 µM forskolin for 1 hour with or without H89 pretreatment. Nuclei were stained with DAPI (blue). Slides were examined by confocal microscopy. Original magnification: 600×, oil. Scale bar: 50 µm. (**H**) Western blot analysis of CREB and p-CREB in ARPE-19 cells treated with 10 ng/mL TGF-β1 for the indicated times with or without 1-hour H89 pretreatment. Gapdh was used for normalization.

Investigative Ophthalmology & Visual Science

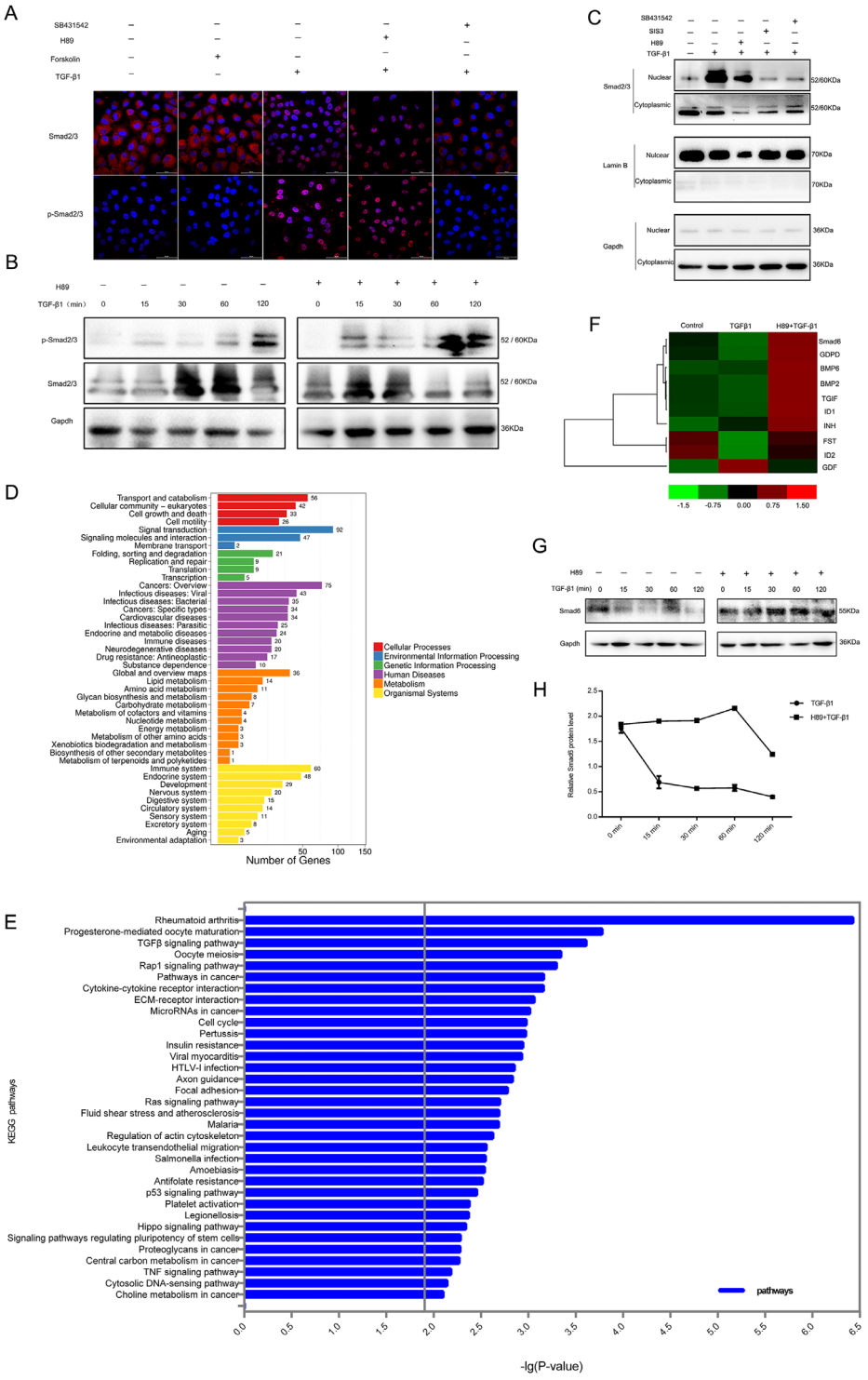

Figure 6. TGF-β-induced PKA activation was dependent on Smad6 but not Smad2/3. (**A**) Immunofluorescence analysis of Smad2/3 and p-Smad2/3 in ARPE-19 cells treated with 10 ng/mL of TGF-β1 or 10 µM forskolin for 1 hour with or without 1-hour pretreatment of H89 or SB431542. Nuclei were stained with DAPI (blue). Slides were examined by confocal microscopy. Original magnification: 600×, oil. Scale bar: 50 µm. (**B**) Western blot analysis of Smad2/3 and p-Smad2/3 in ARPE-19 cells treated with 10 ng/ml TGF-β1 for the indicated times with or without 1-hour H89 pretreatment. Gapdh was used for normalization. (**C**) Nucleocytoplasmic separation for Smad2/3. ARPE-19 cells were treated with TGF-β1 (10 ng/µL) for 30 minutes with or without the pretreatment with H89 (10 µM), SIS3 (10 µM), or SB431542 (0.6 µM). Gapdh was used as a cytoplasmic control and laminin B was used as a nuclear control. (**D**) Pathway classification of DEGs. (**E**) Differentially expressed genes in the TGF-β pathway. Each column represents an experimental sample (e.g., Control, TGF-β1 or TGF-β1+H89), and each row represents a gene. (**F**) The functional enrichment results of DEGs in different pathways that were chosen by -log(P value) > 2. Expression differences are shown in different colors. red: high expression; green: low expression. (**G**) Western blot analysis of Smad6 in ARPE-19 cells treated with 10 ng/mL TGF-β1 for the indicated times with or without H89 pretreatment. Gapdh was used for normalization. (**H**) Quantification of Smad6 expression in Western blots based on the grayscale value.

Investigative Ophthalmology & Visual Science

subjected to KEGG analysis. Five hundred and twenty-eight genes showed differential expression of one-fold or greater ($P < 0.05$). The DEGs were grouped by pathways, including cellular processes, environmental information processing, genetic information processing, human disease, metabolism, and organismal systems pathways. Most of them are environmental information processing pathways including signal transduction-related genes (Fig. 6D). When the functionally enriched pathways of the DEGs were filtered with a threshold of -log(P value) >2, 34 pathways were identified (Fig. 6E). Because the top two ranked pathways were not related to the topic of this study, we focused on the third pathway, the TGF-β pathway. A total of 417 DEGs had pathway annotations, including 10 genes in the TGF-β pathway (2.4%). Furthermore, as indicated by the heatmap (Fig. 6F), the most altered gene in the TGF-β pathway was Smad6.

H89 Prevented the Decrease in Smad6 Expression in TGF-β-Treated ARPE-19 Cells

Smad6 is an inhibitory Smad (I-Smad) along with Smad7,[27] and both proteins have been reported to antagonize the TGF-β and/or BMP pathway(s).[28,29] In this study, we found that TGF-β1 treatment significantly downregulated the expression of Smad6, whereas H89 pretreatment effectively prevented this downregulation in TGF-β1-treated ARPE-19 cells (Figs. 6G and 6H). In contrast to Smad6, Smad7 was minimally affected by TGF-β1 treatment (Supplementary Fig. S2). These results further supported the RNA sequencing data and confirmed that the protective effect of H89 against PVR is related to its maintenance of the Smad6 levels rather than its intervention with the Smad2/3 or Smad7 signals.

Discussion

PVR is a serious challenge in ophthalmologic practice because the lack of effective therapy for this severe complication and the limited understanding of its mechanism. PVR is an anomalous wound repair process characterized by the formation of contractile ERMs that influence cellular attachment, migration, proliferation, and ECM deposition. In one major cellular event associated with PVR, large numbers of RPE cells in the ERMs undergo EMT.[30] This complex process involves damage of ischemic tissues, inflammation, production of local factors, and proliferation of several types of cells, including RPE cells, glial cells, and macrophages.[31] Among these cells, RPE cells deserve the most attention.[32] Proliferating factors, such as TGF-β, can trigger EMT in RPE cells,[4,33,34] during which the cells lose their epithelial morphology and acquire a mesenchymal phenotype characterized by an enhanced migratory capacity, invasiveness, resistance to apoptosis, and ECM production.[35,36] Logistically, if one of these changes can be blocked, the PVR process might be able to be stopped or even reversed. Several drugs are currently being tested in clinical trials or in preclinical studies; these drugs mainly include antiproliferative agents,[37] growth factor modulators,[38] and matrix metalloproteinase inhibitors[39] that target different steps of PVR development. The growth factor modulators are the most complex of the drugs because they include p38MAPK inhibitors,[40] caspase 3 activators, cyclic integrin antagonists, and inhibitors of proliferative cell nuclear antigen.[41] Because no clinical effects have been confirmed, we believed that there might be another signaling pathway or mechanism involved in PVR development. In one of our previous studies on RPE cell differentiation, we observed that treatment with the PKA inhibitor H89 induced differentiation of dedifferentiated ARPE-19 cells in culture and inhibited their EMT. Considering the role of RPE cell EMT in PVR development, we proposed that PKA might be a key factor involved in PVR pathogenesis and that a PKA inhibitor, such as H89, could be a potential drug for the treatment of PVR. This study aimed to confirm this hypothesis and reveal the underlying mechanism.

A basic condition for our hypothesis was the presence and increased activity of PKA in ERMs from patients with PVR. Indeed, in the present study, the PKA pathway was found to be activated in ERMs from patients with PVR. Furthermore, PRKACα, a C subunit of PKA, was confirmed to colocalize with the EMT marker α-SMA and the epithelial marker cytokeratin 8 (Fig. 1). PKA, also known as cAMP-dependent protein kinase, is a heterotetrameric holoenzyme consisting of two regulatory (R) subunits and two C subunits.[42,43] When cAMP levels increase, the active C subunits are released and bind to the two R subunits. Then, the dissociated, active C subunits phosphorylate the serine or threonine residues on a wide variety of proteins.[11] Many effects have been ascribed to PKA, including cell growth, differentiation, ECM production and apoptosis,[12,13] whereas many of these cellular effects are similar to those elicited by TGF-β.

Following a logical progression, we next used H89, a specific PKA inhibitor, to further confirm the potential role of PKA in PVR pathogenesis. Because of ethical issues, our studies were conducted in an animal model and a cultured cell model. As expected, H89 attenuated experimental PVR both in vivo and in vitro. In fact, in PVR model rats, H89 attenuated PVR, protected visual function, and alleviated EMT and ERM formation. The evidence included improvements in b-wave amplitudes in ERG recordings, alleviation of retinal damage and inhibition of EMT marker upregulation (Figs. 2 and 3). In the ARPE-19 cell model, H89 similarly inhibited EMT and ERM formation, attenuated TGF-β-induced RPE migration and collagen gel contraction, and inhibited TGF-β1-induced PKA pathway activation. Based on these observations, we are confident that the PKA pathway is involved in the pathogenesis of PVR, and H89 should be able to delay and alleviate PVR development.

The rat PVR model used in this study is not the only possible model. Various methods can be used to establish in vivo PVR models, including injection of different cells,[44–46] surgical manipulation,[47,48] and intravitreal dispase treatment.[49] Notably, mature RPE cells are mitotically quiescent under normal conditions; only when the neural retina suffers injury do RPE cells start to lose their epithelial morphology, migrate into the vitreous humor, proliferate and participate in the formation of ERMs while undergoing EMT.[4] Therefore, in this study, we used a previously reported rat model with a modification: both ARPE-19 cells and PRP[23] were injected intravitreally. We chose to make this modification because the response and transformation of RPE cells play key roles in PVR pathogenesis and since some factors in PRP could expedite the effects of RPE cells. This model at least partially mimics the pathology of PVR and can achieve a higher success rate (22/26, 84.61%) than the previous PVR model, as confirmed by fundus photographs (Fig. 2). This modified method was also easy and cost-effective.

In addition to cell proliferation, numerous growth factors and cytokines are involved in PVR pathogenesis.[50] TGF-β,

Investigative Ophthalmology & Visual Science

a potent fibrotic factor, is the most crucial player in PVR. The levels of TGF-β have been reported to be elevated in the vitreous humor, subretinal fluid, and proliferative membranes in patients with PVR.[51] Some recently proposed approaches for inhibiting EMT in the context of PVR also target the TGF-β signaling pathway, either by inhibiting TGF-β receptor 1 with LY-364947 [38] or by blocking the nuclear translocation of Smads in ARPE-19 cells with pirfenidone.[52] TGF-β2 has also been used to activate p38MAPK, which is believed to trigger the transcription of Smad 2/3.[48] However, simple inhibition of p38MAPK has not yet been determined to be safe or effective enough for clinical trials, even after many years. In this study, we focused on TGF-β1-related events and observed that the PKA pathway was activated by TGF-β1 treatment, as demonstrated by the translocation of the PKA catalytic subunits into the nucleus, the phosphorylation of CREB and the increased activity of PKA (Fig. 5). However, H89 blocked this TGF-β-induced PKA activation (Fig. 5). These results further indicate that PKA activation in PVR pathogenesis might involve a synergistic effect or crosstalk with the TGF-β pathway.

Considering the important roles of Smad2/3 in the TGF-β superfamily pathway, we examined the effects of the PKA inhibitor H89 on the TGF-β-related canonical Smad2/3 pathway in an in vitro system with ARPE-19 cells. Unexpectedly, H89 did not affect the phosphorylation or nuclear translocation of Smad2/3 (Fig. 6), indicating that the blockade of TGF-β-induced PKA activation was Smad2/3 independent. We then performed RNA sequencing analyses to further explore the possible mechanism, and KEGG analysis revealed that H89 altered the TGF-β pathway and maintained the expression level of an inhibitory Smad, Smad6 (Fig. 6). In fact, we detected changes in both Smad6 and Smad7, the two inhibitory Smads. The results showed that TGF-β1 significantly downregulated Smad6 expression, whereas H89 pretreatment blocked the effect of TGF-β1 on Smad6, maintaining Smad6 at a constant level (Fig. 6). In contrast, both TGF-β1 treatment and H89 pretreatment minimally affected the level of Smad7 (Supplementary Fig. S2). Smads, or SMA and mothers against decapentaplegic-related proteins, are intracellular components of the TGF-β signaling pathway. Among the eight Smads in mammalian species, five are receptor-regulated Smads (R-Smads), including Smad1/2/3/5/9; one is a common Smad (Co-Smad), Smad4; and two are inhibitory Smads (I-Smads), Smad6 and Smad7.[27] The inhibitory Smads can antagonize TGF-β and/or BMP signaling in vitro.[28,53] In previous studies, Smad6 has been reported to be a negative regulator of EMT, and its overexpression decreases EMT progression in the atrioventricular cushion[29] and inhibits epithelial cell activation in the proepicardium.[54] In the eye, Smad6 has been found to play a role in maintaining the lens epithelial phenotype, and its downregulation in β1-integrin-null lenses is related to EMT.[55] Smad6 seemed to play a negative role in EMT in all these reports. In this study, Smad6 was demonstrated for the first time to play a negative role in PVR pathogenesis, and the PKA inhibitor H89 was shown to increase Smad6 expression, thus explaining why it attenuated PVR. The selective PKA inhibitor H89 enhanced the inhibitory role of Smad6. Therefore, in the context of TGF-β-induced EMT or PVR, there may be direct or indirect crosstalk between the PKA pathway and the inhibitory Smad6, but not between the PKA pathway and Smad2/3.

Collectively, these results indicated that PKA pathway activation played important roles in PVR pathogenesis and the PKA inhibitor H89 attenuated experimental PVR both in vivo and in vitro. The mechanism might involve upregulation of Smad6 as a negative EMT regulator and blockade of TGF-β-induced PKA pathway activation. Selective PKA inhibitors are worthy of further study as new therapeutic agents for PVR.

Acknowledgments

Supported by grants obtained from the Ministry of Science and Technology of China (2017YFA0104100, 2015CB964601, 2016YFA0101302), National Natural Science Foundation (81670867, 81372071, 81770942) and Shanghai Municipal Commission of Health and Family Planning project (201640229), Shanghai Science and Technology Committee Grant (17ZR1431300), Shanghai Science and Technology Committee (18411953400) as well as a grant from Shanghai East Hospital ZJ2014-ZD-002.

Author contributions: YL, LL, WL and GX conceived, developed, and mentored the project. YL, WX, JZ, QX, YL, TT, ML and QO performed the experiments. JZ, HT, JX, CJ, FG, JW and AR provided technical and material support. YL, LL and GX analyzed the data. YL, LL and GX wrote the manuscript. All authors read and approved the final manuscript.

Disclosure: **Y. Lyu**, None; **W. Xu**, None; **J. Zhang**, None; **M. Li**, None; **Q. Xiang**, None; **Y. Li**, None; **T. Tan**, None; **Q. Ou**, None; **J. Zhang**, None; **H. Tian**, None; **J.-Y. Xu**, None; **C. Jin**, None; **F. Gao**, None; **J. Wang**, None; **W. Li**, None; **A. Rong**, None; **L. Lu**, None; **G.-T. Xu**, None

References

1. Pastor JC, Rojas J, Pastor-Idoate S, et al. Proliferative vitreoretinopathy: a new concept of disease pathogenesis and practical consequences. *Prog Retin Eye Res*. 2016;51:125–155.
2. Di Lauro S, Kadhim MR, Charteris DG, Pastor JC. Classifications for proliferative vitreoretinopathy (PVR): an analysis of their use in publications over the last 15 years. *J Ophthalmol*. 2016. 2016:7807596.
3. Kaneko H, Terasaki H. Biological involvement of MicroRNAs in proliferative vitreoretinopathy Kaneko and Terasaki. *Translational Vision Science & Technology*. 2017;6(4):5–5.
4. Chiba C. The retinal pigment epithelium: An important player of retinal disorders and regeneration. *Experimental Eye Research*. 2014;123(Supplement C):107–114.
5. Palomares-Ordonez JL, ánchez-Ramos JA, Ramírez-Estudillo JA, Robles-Contreras A. Correlation of transforming growth factor beta-1 vitreous levels with clinical severity of proliferative vitreoretinopathy in patients with rhegmatogenous retinal detachment. *Arch Soc Esp Oftalmol*. 2019;94:12–17.
6. Kumar A, Li X. PDGF-C and PDGF-D in ocular diseases. *Mol Aspects Med*. 2018;62:33–43.
7. Hoerster R, Fauser S, Cursiefen C, Kirchhof B, Heindl LM. The influence of systemic renin-angiotensin-inhibition on ocular cytokines related to proliferative vitreoretinopathy. *Graefes Arch Clin Exp Ophthalmol*. 2017;255:1721–1725.
8. Ciprian D. The pathogeny of proliferative vitreoretinopathy. *Rom J Ophthalmol*. 2015;59:88–92.
9. Wang L, Dong F, Reinach PS, et al. MicroRNA-182 suppresses HGF/SF-induced increases in retinal pigment epithelial cell proliferation and migration through targeting c-Met. *PLoS One*. 2016;11:e0167684.
10. Du Y, Chen Q, Huang L, et al. VEGFR2 and VEGF-C suppresses the epithelial-mesenchymal transition via YAP in retinal pigment epithelial cells. *Curr Mol Med*. 2018;18:273–286.

11. Taylor SS, Buechler JA, Yonemoto W. cAMP-dependent protein kinase: framework for a diverse family of regulatory enzymes. *Annu Rev Biochem*. 1990;59:971–1005.
12. McKnight GS, Cummings DE, Amieux PS, et al. Cyclic AMP, PKA, and the physiological regulation of adiposity. *Recent Prog Horm Res*. 1998;53:139–159; discussion 160-1.
13. Walsh DA, Van Patten SM. Multiple pathway signal transduction by the cAMP-dependent protein kinase. *Faseb J*. 1994;8:1227–1236.
14. Kreisberg JI, Radnik RA, Kreisberg SH. Phosphorylation of cAMP responsive element binding protein after treatment of mesangial cells with high glucose plus TGFβ or PMA. *Kidney International*. 1996;50:805–810.
15. Wang L, Zhu Y, Sharma K. Transforming growth factor-beta1 stimulates protein kinase A in mesangial cells. *J Biol Chem*. 1998;273:8522–8527.
16. Kramer IM, Koornneef I, de Laat SW, van den Eijnden-van Raaij AJ. TGF-beta 1 induces phosphorylation of the cyclic AMP responsive element binding protein in ML-CCl64 cells. *Embo J*. 1991;10:1083–1089.
17. Potchinsky MB, Weston WM, Lloyd MR, Greene RM. TGF-beta signaling in murine embryonic palate cells involves phosphorylation of the CREB transcription factor. *Exp Cell Res*. 1997;231:96–103.
18. Yang Y, Pan X, Lei W, et al. Regulation of transforming growth factor-beta 1-induced apoptosis and epithelial-to-mesenchymal transition by protein kinase A and signal transducers and activators of transcription 3. *Cancer Res*. 2006;66:8617–8624.
19. Yang H, Lee CJ, Zhang L, Sans MD, Simeone DM. Regulation of transforming growth factor beta-induced responses by protein kinase A in pancreatic acinar cells. *Am J Physiol Gastrointest Liver Physiol*. 2008;295:G170–G178.
20. Dean DC, Newby RF, Bourgeois S. Regulation of fibronectin biosynthesis by dexamethasone, transforming growth factor beta, and cAMP in human cell lines. *J Cell Biol*. 1988;106:2159–2170.
21. Peng F, Zhang B, Wu D, Ingram AJ, Gao B, Krepinsky JC. TGFbeta-induced RhoA activation and fibronectin production in mesangial cells require caveolae. *Am J Physiol Renal Physiol*. 2008;295:F153–F164.
22. Chowdhury S, Howell GM, Rajput A. Identification of a novel TGFbeta/PKA signaling transduceome in mediating control of cell survival and metastasis in colon cancer. *PLoS One*. 2011;6:e19335.
23. Zheng XZ, Du LF, Wang HP. An immunohistochemical analysis of a rat model of proliferative vitreoretinopathy and a comparison of the expression of TGF-beta and PDGF among the induction methods. *Bosn J Basic Med Sci*. 2010;10:204–209.
24. Zhao HM, Sheng MJ, Yu J. Expression of IGFBP-6 in a proliferative vitreoretinopathy rat model and its effects on retinal pigment epithelial cell proliferation and migration. *Int J Ophthalmol*. 2014;7:27–33.
25. Metzger H, Lindner E. The positive inotropic-acting forskolin, a potent adenylate cyclase activator. *Arzneimittelforschung*. 1981;31:1248–1250.
26. Callahan JF, Burgess JL, Fornwald JA, et al. Identification of novel inhibitors of the transforming growth factor beta1 (TGF-beta1) type 1 receptor (ALK5). *J Med Chem*. 2002;45:999–1001.
27. Li Q. Inhibitory SMADs: potential regulators of ovarian function. *Biol Reprod*. 2015;92:50.
28. Imamura T, Takase M, Nishihara A, et al. Smad6 inhibits signalling by the TGF-beta superfamily. *Nature*. 1997;389:622–626.
29. Desgrosellier JS, Mundell NA, McDonnell MA, Moses HL, Barnett JV. Activin receptor-like kinase 2 and Smad6 regulate epithelial-mesenchymal transformation during cardiac valve formation. *Dev Biol*. 2005;280:201–210.
30. Begum G, O'Neill J, Chaudhary R, et al. Altered decorin biology in proliferative vitreoretinopathy: a mechanistic and cohort study. *Invest Ophthalmol Vis Sci*. 2018;59(12):4929–4936.
31. Garweg JG, Tappeiner C, Halberstadt M. Pathophysiology of proliferative vitreoretinopathy in retinal detachment. *Surv Ophthalmol*. 2013;58:321–329.
32. Campochiaro PA. Pathogenic mechanisms in proliferative vitreoretinopathy. *Arch Ophthalmol*. 1997;115:237–241.
33. Limb GA, et al. Cytokines in proliferative vitreoretinopathy. *Eye (Lond)*. 1991;5:686–693.
34. Baudouin C, Hofman P, Brignole F, Bayle J, Loubière R, Gastaud P. Immunocytology of cellular components in vitreous and subretinal fluid from patients with proliferative vitreoretinopathy. *Ophthalmologica*. 1991;203:38–46.
35. Grisanti S, Guidry C. Transdifferentiation of retinal pigment epithelial cells from epithelial to mesenchymal phenotype. *Investigative Ophthalmology & Visual Science*. 1995;36(2):391–405.
36. Saika S, Yamanaka O, Okada Y, et al. TGF beta in fibroproliferative diseases in the eye. *Front Biosci (Schol Ed)*. 2009;1:376–390.
37. Pastor JC, Rodríguez E, Marcos MA, Lopez MI. Combined pharmacologic therapy in a rabbit model of proliferative vitreoretinopathy (PVR). *Ophthalmic Res*. 2000;32:25–29.
38. Nassar K, Grisanti S, Tura A, et al. A TGF-beta receptor 1 inhibitor for prevention of proliferative vitreoretinopathy. *Exp Eye Res*. 2014;123:72–86.
39. Ozerdem U, Mach-Hofacre B, Cheng L, et al. The effect of prinomastat (AG3340), a potent inhibitor of matrix metalloproteinases, on a subacute model of proliferative vitreoretinopathy. *Curr Eye Res*. 2000;20:447–453.
40. Saika S, Yamanaka O, Ikeda K, et al. Inhibition of p38MAP kinase suppresses fibrotic reaction of retinal pigment epithelial cells. *Laboratory Investigation*. 2005;85:838–850.
41. Zhang X, Barile G, Chang S, et al. Apoptosis and cell proliferation in proliferative retinal disorders: PCNA, Ki-67, caspase-3, and PARP expression. *Curr Eye Res*. 2005;30:395–403.
42. Lao VV, Grady WM. Epigenetics and colorectal cancer. *Nat Rev Gastroenterol Hepatol*. 2011;8:686–700.
43. Potter RL, Stafford PH, Taylor S. Regulatory subunit of cyclic AMP-dependent protein kinase I from porcine skeletal muscle: purification and proteolysis. *Archives of Biochemistry and Biophysics*. 1978;190:174–180.
44. Sugita G, Tano Y, Machemer R, Abrams G, Claflin A, Fiorentino G. Intravitreal autotransplantation of fibroblasts. *Am J Ophthalmol*. 1980;89:121–130.
45. Radtke ND, Tano Y, Chandler D, Machemer R. Simulation of massive periretinal proliferation by autotransplantation of retinal pigment epithelial cells in rabbits. *Am J Ophthalmol*. 1981;91:76–87.
46. Hui YN, Goodnight R, Sorgente N, Ryan SJ. Fibrovascular proliferation and retinal detachment after intravitreal injection of activated macrophages in the rabbit eye. *Am J Ophthalmol*. 1989;108:176–84.
47. Cleary PE, Ryan SJ. Vitrectomy in penetrating eye injury. Results of a controlled trial of vitrectomy in an experimental posterior penetrating eye injury in the rhesus monkey. *Arch Ophthalmol*. 1981;99:287–292.
48. Saika S, Kono-Saika S, Tanaka T, et al. Smad3 is required for dedifferentiation of retinal pigment epithelium following retinal detachment in mice. *Lab Invest*. 2004;84:1245–1258.
49. Kralinger MT, Kieselbach GF, Voigt M, et al. Experimental model for proliferative vitreoretinopathy by intravitreal dispase: limited by zonulolysis and cataract. *Ophthalmologica*. 2006;220:211–216.

Investigative Ophthalmology & Visual Science

50. Cui JZ, Chiu A, Maberley D, Ma P, Samad A. Stage specificity of novel growth factor expression during development of proliferative vitreoretinopathy. *Eye (Lond)*. 2007;21:200–208.
51. Connor TB, Jr, Roberts AB, Sporn MB, et al. Correlation of fibrosis and transforming growth factor-beta type 2 levels in the eye. *J Clin Invest*. 1989;83:1661–1666.
52. Choi K, Lee K, Ryu SW, Im M, Kook KH, Choi C. Pirfenidone inhibits transforming growth factor-beta1-induced fibrogenesis by blocking nuclear translocation of Smads in human retinal pigment epithelial cell line ARPE-19. *Mol Vis*. 2012;18:1010–1020.
53. Nakao A, Afrakhte M, Morén A, et al. Identification of Smad7, a TGFbeta-inducible antagonist of TGF-beta signalling. *Nature*. 1997;389:631–635.
54. Olivey HE, Mundell NA, Austin AF, Barnett JV. Transforming growth factor-beta stimulates epithelial-mesenchymal transformation in the proepicardium. *Dev Dyn*. 2006;235:50–59.
55. Simirskii VN, Wang Y, Duncan MK. Conditional deletion of beta1-integrin from the developing lens leads to loss of the lens epithelial phenotype. *Dev Biol*. 2007;306:658–668.

Investigative Ophthalmology & Visual Science